Single-Layer graphene growth on crystalline Ni(111) and Ni(110) and the fate of Carbon on crystalline Ni(100)

Daniela L. Mafra[1], Jimena A. Olmos-Asar[2,*], Fabio R. Negreiros[2,*], Jimena A. Olmos-Asar[2*], Alfonso Reina[3], Ki Kang Kim[4], Mildred S. Dresselhaus[1,5], Jing Kong[1] and Paulo T. Araujo[6,7,*]

[1]Department of Electrical Engineering and Computer Sciences, Massachusetts Institute of Technology, Cambridge, Massachusetts 02139, USA.
[2]Centro de Ciências Naturais e Humanas, Universidade Federal do ABC, Santo André, 09210-580 SP, Brazil.
[3]Department of Materials Science and Engineering, Massachusetts Institute of Technology, Cambridge, Massachusetts 02139, USA.
[4]Department of Energy and Materials Engineering, Dongguk University-Seoul, Seoul, 04620, Republic of Korea.
[5]Department of Physics, Massachusetts Institute of Technology, Cambridge, Massachusetts 02139, USA.
[6]Department of Physics and Astronomy, The University of Alabama, Tuscaloosa, Alabama 35487, USA.
[7]Center for Materials for Information Technology (MINT Center), The University of Alabama, Tuscaloosa, USA.

PHYSICAL SCIENCES: Applied Physical Sciences; Engineering.

KEY WORDS: Chemical Vapor Deposition, Graphene, Nickel, Diffusion, Segregation.

ABSTRACT

The growth of large area single-layer graphene (1-LG) is studied using ambient pressure CVD on single crystal Ni(111), Ni(110) and Ni(100). By varying both the furnace temperature in the range of 800 - 1100 ^{o}C and the gas flow through the growth chamber, a uniform growth of high-quality 1-LG is obtained for Ni(111) and Ni(110), but only multilayer graphene (M-LG) growth could be obtained for Ni(100), except for Ni(100) thin films, in which 1-LG is successfully grown The experimental results are interpreted to obtain the optimum combination of temperature and gas flow. Characterization with optical microscopy, Raman spectroscopy and optical transmission accordingly support our findings. DFT calculations are performed to elucidate our results through different thermodynamic and kinetic mechanisms, such as diffusion, segregation and adsorption, which dictate the formation of different carbon structures over the different crystallographic directions of Ni.

INTRODUCTION

The growth of carbon structures over different metallic/semi-metallic substrates has been extensively studied in the past decades [1-50]. A great deal of attention has been devoted mainly to Nickel (Ni) substrates in their several different crystallographic directions [1-27, 43-46]. These previous works reported the formation of different carbon structures (including single-layer graphene - 1-LG) over the three different low index crystallographic orientations of the Ni substrates (Ni(111), Ni(110) and Ni(100)). However, an understanding of how to combine different thermodynamic parameters to assure the formation of high quality carbon layers, regardless of the Ni substrate crystallographic direction, is only partially understood [15, 16, 30, 31, 46, 47, 51-57]. Indeed, some works in the literature report the growth of 1-LG on Ni(111)

and Ni(110), but authors address the same explanations for the growth mechanisms in those directions even though the (111) and the (110) directions have distinctly different thermodynamic properties [1-27, 30, 31, 43-47, 51-57]. With the advances in 1-LG growth techniques boosted by the isolation of 1-LG from a bulk graphite substrate [28], recent research has shown the possibility of growing 1-LG and multi-layer graphene (M-LG) over metals using the CVD technique without ultra-high vacuum environments and subsequently transferring such a material to a diversity of dielectric substrates [7-19, 29-32, 54-57]. The combination of process flexibility and high quality of the material produced from these fabrication processes has enabled the integration of graphene into various applications [33, 43-47, 51-57].

Although graphene has been grown successfully over various transition metals, copper (Cu) and nickel (Ni) are the cheapest and most widely used substrates [9, 43-47, 51-57]. Copper is the most frequently used metal to grow monolayer graphene, since the low carbon solubility in Cu leads to a desirable self-limiting surface growth of graphene [19, 32]. The same is not true for nickel (Ni), because carbon dissolution into the bulk at typical high growth temperatures can result in a high rate of carbon segregation and M-LG formation upon cooling. On the other hand, the growth of 1-LG on Cu, in general, needs to be carried out under low pressure [34], which complicates the synthesis process and adds to the cost of graphene production. Nickel has some advantages over copper insofar as the growth of M-LG can be avoided. For example, due to a stronger interaction between graphene and Ni, only one graphene-domain-orientation exists for graphene growth on Ni(111) single crystal, and therefore, no tilt-grain boundaries are expected, after a continuous and high-quality film of graphene is formed [35].

It is worth mentioning that the mechanisms behind the growth of 1-LG on Ni are different from those mechanisms behind the growth of 1-LG on Cu. In short, the growth of 1-LG in Cu is mainly mediated by the adsorption of carbon atoms by the surface atoms followed by the diffusion of such atoms across the surface and the formation of nucleation centers [34, 43-47, 51-57]. In Ni, however, diffusion (segregation) into (from) the bulk as well as epitaxial growth mediated by nucleation centers are of major importance [1-5, 30, 34, 40, 41, 43-47, 51-57]. Moreover, it is significant to point out that the growth of 1-LG graphene over Ni is a prime step toward the controlled growth of high-quality multi-layer graphene that is also important for a number of technological applications [43-47, 51-57]. As an example, Seah et al. have recently demonstrated the growth of bilayer graphene (2-LG) on Ni(111) by controlling the cooling temperature, which in turn controls the rates of carbon segregation [56].

In this work, we show that using Ni in single crystal form with different crystallographic orientations (Ni(111), Ni(110) and Ni(100)), it is possible to obtain uniform 1-LG employing ambient pressure CVD. We characterize the different growth mechanisms found on each orientation with optical microscopy, Raman spectroscopy and optical transmission. DFT calculations are also performed to provide an atomistic model of the processes involved; this further supports the experimental results. It is found that the formation of a uniform monolayer over Ni single crystal substrates is epitaxially driven in the (111) direction, while it happens due to surface thermodynamics and kinetic effects in the (110) and (100) cases, mostly in terms of the diffusion and segregation of carbon atoms over Ni surfaces [2, 3, 5, 20]. The results and

explanations provided by this work could be a first step to control the number of graphene layers formed on the surface.

METHODS

Experimental details

The Ni(111), Ni(110) and Ni(100) single crystals used in this work (10mm in diameter, 1mm thick, 99.9995% purity) were obtained from Marketech International. The Ni(100) thin films are around 1μm thick. Throughout the text, the discussions will consider the 1mm thick crystal except when clearly specified otherwise (as for example in the section "Growth of 1-LG on Ni(100) Thin Films"). The pieces were electro-polished further with a mixing of glacial acetic acid and perchloric acid (60%) in the ratio of 7:3 in volume, respectively, to guarantee a low roughness of the substrates. X-ray diffraction measurements for each Ni piece were taken after the polishing to confirm the crystallographic orientation. The growth of graphene was done under an ambient pressure CVD process, as described below: the CVD process involves the rapid heating of the polished Ni pieces under the flow of hydrogen (1000 sccm). A 1 inch tube furnace is used and it is preheated to the growth temperature (T) before the introduction of a silica tube containing the Ni pieces inside. When the temperature stabilizes back to T, methane gas (100 sccm) is added to the hydrogen flow. Exposure to methane lasts for a time t=5min before taking the silica tube out of the furnace to a room temperature environment for a fast cool down. The transfer of the graphene grown in this way is done using a PMMA layer spin-coated over the Ni surface followed by electrochemical delamination of the graphene/PMMA [48 -50]. The electrolyte consists of a 1M NaOH solution with a negative -10V applied on the Ni. The PMMA/graphene layer detaches from the Ni substrate and it can be placed over a dielectric substrate followed by an acetone removal of the PMMA [17].

Computational details

Density Functional calculations [58] were performed with the Quantum-Espresso Package [59] and the Perdew-Burke-Ernzerhof [60] Generalized Gradient Approximation as exchange correlation functional. The ultrasoft pseudopotentials of the pslibrary [61] were used with plane-wave/charge density energy cutoffs of 40/320 Ry, respectively. The sampling of the first brillouin zone was performed using grids centered at the Γ point, with a k-point density 2x2x1 for the (100) and (110) faces and 2x3x1 for the (111) face. 12 Å of vacuum was added in the perpendicular direction to avoid spurious interaction between periodic images. The energy and force thresholds adopted for the geometry optimizations were 0.0001/0.001a.u., respectively. Van der Waals corrections within the Grimme-2D method [62] were also considered.

RESULTS AND DISCUSSION

Figure 1 shows optical microscopy, AFM and Raman spectroscopy characterization of the 1-LG films obtained for Ni(111) and Ni(110) after transferring the 1-LG films to Si/SiO$_2$ substrates (note that 1-LG in Ni(100) thin films will be discussed later in the text). The optical images (Figures 1a and 1b) show a uniform contrast in a similar way as obtained for samples derived from Cu foils [17-19, 23]. The observed optical color contrast corresponds to the one estimated

for 1-LG under the same theoretical model as was described previously [23]. The cross sectional thickness of the film is estimated from the AFM tapping mode image to range from 0.48 to 0.57 nm (Figures 1c and 1d), which is in the expected range for a 1-LG sample. Raman spectroscopy (Figures 1e and 1f) confirms the presence of graphitic carbon in its monolayer configuration. Three main features are observed with 532 nm laser wavelength excitation; the D, G, and 2D Raman peaks around 1350 cm^{-1}, 1580 cm^{-1} and 2700 cm^{-1}, respectively. The intensity ratio between the 2D and G peak intensities (I_{2D}/I_G) close to 2 and the full width at the half maximum (FWHM) of the 2D band which is ~ 30 cm^{-1} are spectroscopic signatures of the presence of 1-LG. Further confirmation of the presence of 1-LG and of its quality when grown on Ni(111) and Ni(110) catalysts was done by measuring the optical transmittance of the films over the visible range (Figure 2d). The films were also transferred to quartz substrates and the average transmittance was measured to be around 97.8% for 1-LG grown on both Ni(111) and Ni(110), which is within experimental error when compared to the transmission expected for 1-LG (97.7%) [23]. The transmittance was also found to be similar to that measured for 1-LG grown over a Cu foil following the growth process described elsewhere [36, 37].
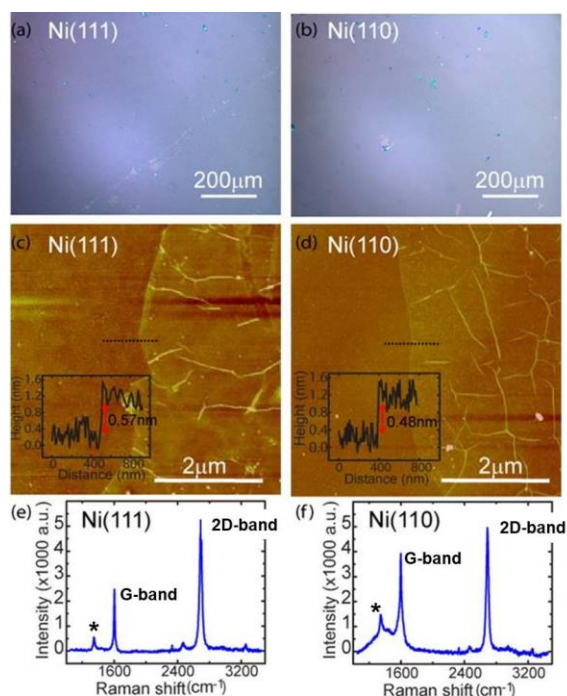

Figure 1| (a) and (b) show the optical microscopy image of 1-LG grown on Ni(111) and on Ni(110), respectively, after transferring the 1-LG layer to the Si/SiO$_2$ substrate. (c) and (d) show the AFM image of the edge of a typical 1-LG graphene film deposited on the Si-SiO$_2$ substrate for 1-LG grown on Ni(111) and Ni(110), as labelled. The insets, containing information on the sample profile, reveal that for both cases, Ni(111) and Ni(110), 1-LG is indeed formed. Finally, (e) and (f) show the Raman spectra for the 1-LG grown on Ni(111) and Ni(110), respectively. The asterisk stands for D-band, a disorder-related Raman

Here, we report some process parameters that are of significant importance for the success of 1-LG growth on Ni(111) and Ni(110) single crystals. First, as illustrated in Figure 2f, polishing the surface of Ni pieces (as described in the Methods section) was critical for 1-LG preparation due to the observed formation of M-LG under the same processing conditions on samples rougher than a few nanometers (Root Mean Squared - RMS). Figures 2(a) through (c) show Atomic Force Microscopy (AFM) images of clean and polished surfaces for Ni(111) (a), Ni(100) and Ni(110) before graphene growth. The surface roughness is the largest for Ni(110) and the smallest for Ni(111). No surface was rough enough to prevent monolayer growth. Such a formation of M-LG can be attributed to the well-known preference of graphene formation on Ni step edges, which are abundant in grooves and features making up a rough crystalline surface [25, 38, 39], inducing the overlap of continuous neighboring growing graphene islands [1-5, 35, 38]. The inset in Figure 2f shows the X-Ray Diffraction (XRD) measurements taken from the Ni(111), Ni(110) and Ni(100) single crystals, confirming their crystallographic directions.
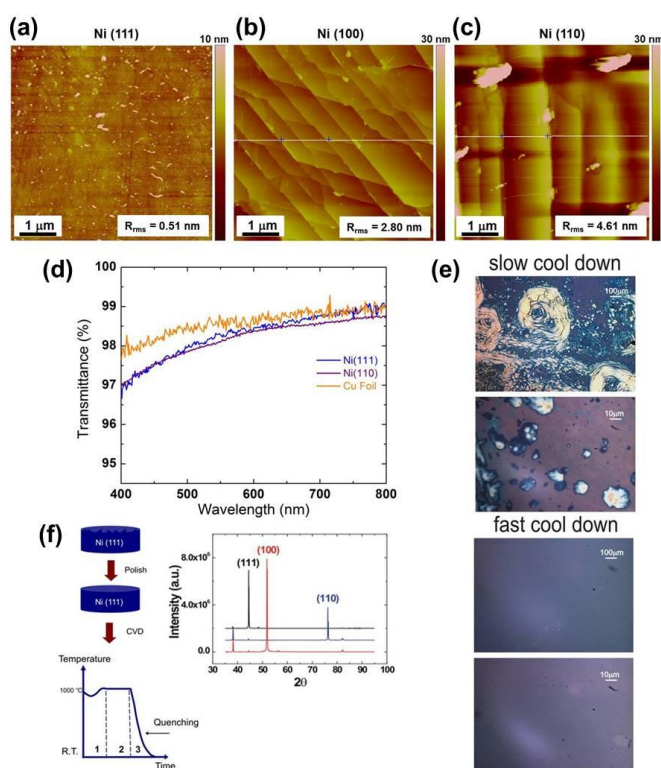

Figure 2| Atomic Force Microscopy (AFM) images of clean and polished surfaces for Ni(111) (a), Ni(100) and Ni(110) before graphene growth. (d) Optical transmittance across the wavelength range of 400-800

nm for 1-LG films grown from Ni(111) (blue), Ni(110) (purple) and Cu foil (orange). (e) Images of samples obtained for Ni(111) using fast and slow cool down approaches starting at T=1000 ^{o}C. Through the optical images we can see that using fast quenching we get a very continuous film of 1-LG, while using slow quenching most parts of the graphene film are not homogeneous and are composed of few layer flakes and fragments. (f) Schematic of the processing steps for growing 1-LG from Ni single crystal. The inset shows the XRD measurements taken from the Ni(111), Ni(110) and Ni(100) single crystals confirming their crystallographic directions.

Second, the speed in which the temperature quenching of the Ni pieces is performed plays a significant role in the crystalline structure of the resulting sample. Using a fast cool down is very important to get 1-LG, since it prevents the formation of a graphite phase after the monolayer forms over the Ni surface (bottom panel in Figure 2e). Slow quenching results in films formed mostly by M-LG (top panel in Figure 2c). Last, the growth temperature (T) is fundamental to achieve 1-LG formation on Ni. For the same gases and flow rates (H$_2$=1000 sccm, CH$_4$=100 sccm) and growth time (t=5 min), the growth temperature T was found to be specific for each Ni single crystal orientation. We found that 1-LG on Ni(111) is formed using T=(1000±1) ^{o}C. At this temperature, Ni(110) and Ni(100) give M-LG, as shown in Figures 3d, 3e and 3f. For T=(800±1) ^{o}C , we obtain 1-LG on Ni(110) and M-LG for Ni(111) and Ni(100), as shown in Figures 3g, 3h and 3i. For the experimental conditions investigated in this work, we could not obtain formation of 1-LG on Ni(100), except when Ni(100) thin films were considered. For T<800 ^{o}C, no carbon structures were formed on the Ni surfaces, independent of their crystallographic orientation. Table 1 summarizes these results for 1mm thick Ni crystals.
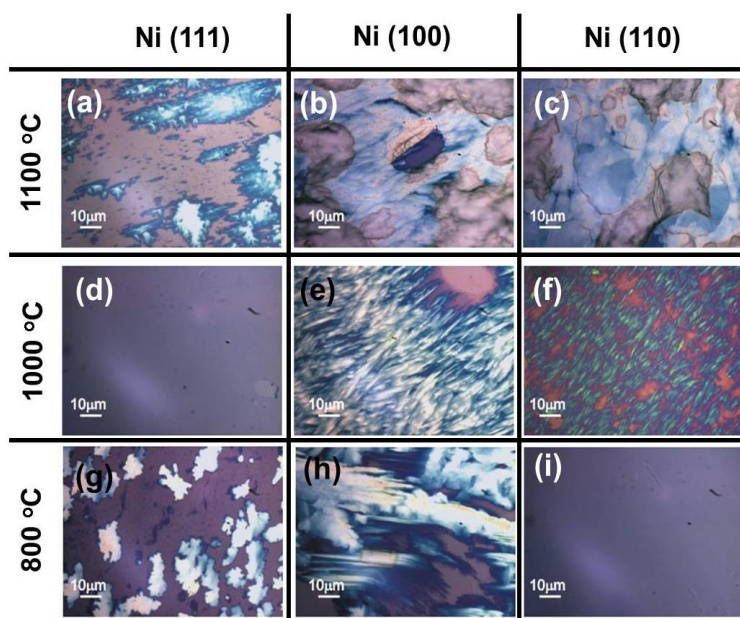

Figure 3| Optical absorption images of graphene grown on the (111), (100) and (110) Ni faces at temperatures of 800, 1000 and 1100 ^{o}C. Multi-layer graphene pieces are obtained in all cases, except Ni(110) at 800 ^{o}C (i) and Ni(111) at 1000 ^{o}C (d), where a 1-LG is obtained.

Table 1| Results for the growth of carbon structures at different temperatures and different crystallographic directions. 1-LG stands for single-layer graphene and M-LG stands for multi-layer graphene. Gas flow rates: H_2=1000 sccm and CH_4=100 sccm.

	Ni(111)	Ni(110)	Ni(100)
1100 ^{o}C	M-LG	M-LG	M-LG
1000 ^{o}C	1-LG	M-LG	M-LG
800 ^{o}C	M-LG	1-LG	M-LG
<800 ^{o}C	None	None	None

Growth of 1-LG on Ni(111):

Nickel crystals are Face Centered Cubic (FCC) structures with a bulk lattice parameter of 3.52 Å. Ni(111) has a surface lattice parameter of $a_{Ni(111)}$ = 2.49 Å, which is very close to that of 1-LG, a_{1-LG} = 2.46 Å [1-5]. Moreover, when compared to the other two directions Ni(110) and Ni(100), Ni(111) has the highest atomic packing density [41, 63] and the smallest surface energy, $S_{Ni(111)}$ = 1606 ergs.cm^{-2} against $S_{Ni(110)}$ = 2057 ergs.cm^{-2} and $S_{Ni(100)}$ = 1943 ergs.cm^{-2} [1-5, 64]. Since the surface energy is related to the strength of the C-Ni interaction, we expect that the carbon adsorption energy and energy barriers E_{across} for the diffusion across the bulk surface [40-42, 65] to be related to $S_{Ni(111)}$, which means that they should be lower in this (111) face. Diffusion of carbon atoms will also be dependent on its surface mean-free path. Indeed, if the density of C atoms increases, the mean free path decreases, which makes diffusion less likely. Additionally, the C deposition rate $R_{Ni(111)}$, which is proportional to the reactivity rate of methane (CH_4) on that surface, is the smallest on this face, at any temperature [1-5].

In our experiments, for this Ni(111) crystallographic direction, by keeping the gas flow of H_2 and CH_4 at 1000 sccm and 100 sccm, respectively, and a fast cooling down of the sample, 1-LG was obtained at (1000±1) ^{o}C, while M-LG was obtained at (1100±1) ^{o}C and at (800±1) ^{o}C and no carbon structure formation was observed for temperatures below (800±1) ^{o}C (we have studied temperatures between 750 ^{o}C and 800 ^{o}C in steps of 10 ^{o}C). Therefore, the temperature of (1000±1) ^{o}C is the optimum temperature that balances the main driving phenomena behind the growth mechanism: deposition rate, diffusion across the bulk surface, diffusion into the bulk and fast cool down segregation. One could also argue that the temperature of 1000 ^{o}C is also important because it increases the CH_4 reactivity. Indeed, there is an increase in the CH_4 reactivity at higher temperatures, but this should not be the main reason because already at 800 ^{o}C this reactivity is high enough to lead to M-LG formation (see Table 1).

7

At 800 ^{o}C, diffusion into the bulk must decrease sensitively compared to 1000 ^{o}C and, consequently, the segregation during the fast cool down must be even harder. Indeed, the diffusion of carbon atoms into the bulk at 1000 ^{o}C and the low segregation at fast cool down rates are what controls the density of carbon atoms at the Ni(111) surface, thereby allowing 1-LG formation. We also understand that at higher temperatures such as 1100 ^{o}C, the probability of carbon atom diffusion across the surface and the probability of carbon atom diffusion into the bulk are approximately equivalent and the density of carbon atoms that diffuse into the bulk is even larger than the diffusion into the bulk at 1000 ^{o}C. The sample at 1100 ^{o}C takes longer to cool down, which results in a high rate of carbon atom segregation during the cooling down process, and thus M-LG was preferentially obtained on Ni(111).

Provided that we change some parameters during the growth, we also show that for temperatures between 780 ^{o}C and 1000 ^{o}C, the growth of monolayers in Ni(111) is possible. As the temperature is decreased from 1000 ^{o}C, the deposition rate and the sticking coefficient of carbon on the Ni substrate decrease and the fact we are obtaining M-LG between 1000 ^{o}C and 780 ^{o}C probably means that the flow of CH$_4$ is still too high in such cases, even though the deposition rate decreases (diffusion into the bulk is increasingly suppressed as the temperature decreases). Therefore, if one substantially decreases the CH$_4$ flow, 1-LG is expected to be grown. Indeed, we verified this to happen in our experiments, as shown in Figure 4(a)-(c), where we demonstrate that mostly 1-LG can be obtained at 900 ^{o}C if the CH$_4$ flow is reduced from 100 to 50 sccm, while the H$_2$ flow is kept at 1000 sccm, and the fast cool down of the sample is also employed. Figure 4(d) shows the Raman spectrum for the 1-LG grown under such conditions.
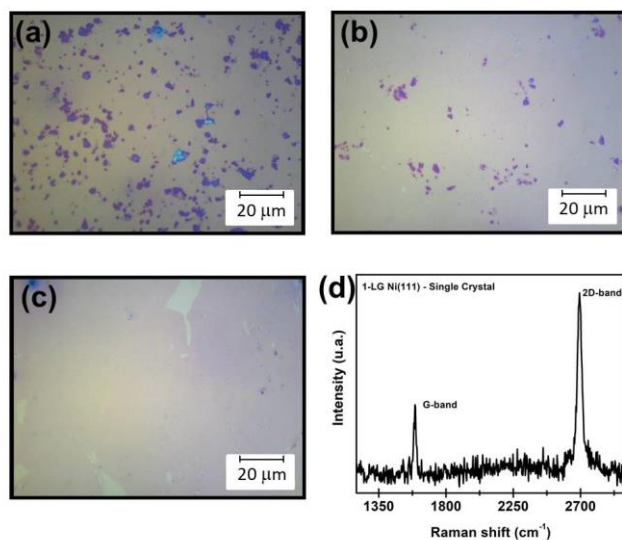

Figure 4| Optical images of the graphene films obtained from Ni(111) at T=900 ^{o}C and gas flows of H$_2$ = 1000 sccm and (a) CH$_4$ = 100 sccm, (b) CH$_4$ = 75 sccm and (c) CH$_4$ 50 sccm. 1-LG is formed when the flow of methane is decreased from 100 sccm to 50 sccm. (d) Raman spectrum for the 1-LG shown in (c).

Our computer simulations suggest that 1LG on Ni(111) has a planar structure, with half of the carbon atoms attached to an on-top position and the other half attached to a hollow-hcp position, as shown in Figure 5. Although we present this structure as the most stable, there is still disagreement about the best atomic arrangement of graphene on Ni(111). In fact, it has been shown that more than one structures may coexist [9, 66, 67], due to the very low energy difference between them. The structural and energetic parameters are listed in Table 2.
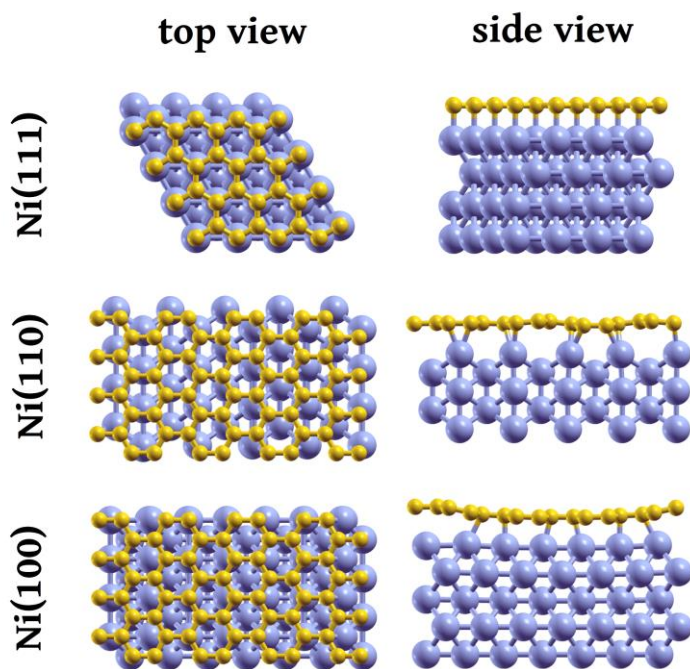

Figure 5 | 1-LG on nickel, in its optimized configuration. In yellow, carbon atoms and in blue, nickel.

Table 2 | Energetic and structural information of 1-LG on different crystal planes as obtained by DFT calculations, as shown in Fig. 05. The values show the average adsorption energy by atom, the average carbon-surface distance and the maximum buckling on the graphene layer.

	E_{ads} (meV.at^{-1})	$d_{graph-surf}$ (Å)	buckling (Å)
Ni(111)	164	2.11	0.00
Ni(110)	209	2.03	0.29
Ni(100)	180	2.13	0.69

Suggested Model for carbon growth on Ni(111):

We have calculated the adsorption energy of a single carbon atom on a perfect Ni(111) surface, emulating the low concentration regime, which corresponds to the first stages of growth (see Figure 6). Nearly all generated carbon will diffuse laterally until it finds another atom to create a dimer (trimers and tetramers are less stable than dimers, so probably the first stages of the growth will involve only dimers). The best site for carbon adsorption on the surface is on a hollow-hcp (for more information about the structures and the way of calculating the adsorption energies, please see the Supporting Material). The carbide position, which corresponds to carbon absorption, is even more stable by 0.42 eV. For a second C atom, there is a 0.33 eV gain in forming a dimer, instead of adsorbing far away from the first C atom. All the adsorption energies for a single carbon atom, as well as the structural parameters for the configurations, are presented in Table S1. To have a whole picture of the processes involved in the first stages of carbon deposition, we have also evaluated the diffusion barriers for some relevant paths: the diffusion across (E_{across}) and into the surface (E_{into}) for a carbon atom, as well as dimer diffusion across the surface. Figure 7a illustrates the main paths considered and Figure 7b quantifies them, from which we extract that the E_{across} barrier is less than half of E_{into}.

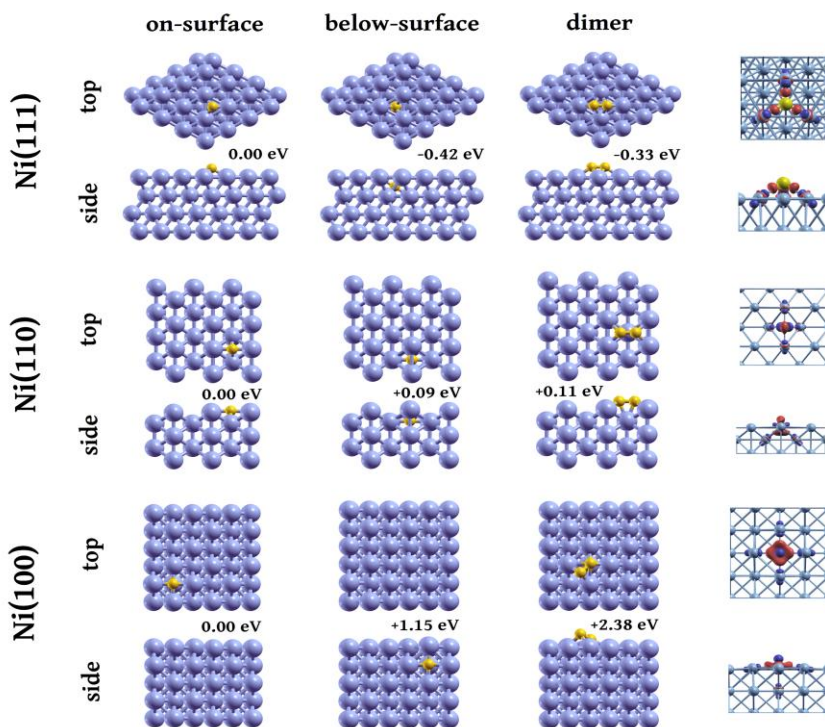**Comment [PA1]:** Is this right?

Figure 6 | The most stable sites for (from left to right): carbon adsorption, carbide formation, and dimer formation on different Ni crystal planes. The color code is the same as in Figure 5. The relative adsorption energies for each surface are displayed, and in the case of dimers, the value corresponds to the energy variation with respect to the adsorption of two isolated C atoms. On the right, the charge density

difference for single atom adsorption is shown. In these plots, red/blue means electron accumulation/depletion.

With these experimental and theoretical results in mind, we propose a possible scenario for graphene formation on Ni(111). At the low coverage regime, the incoming C atoms should adsorb at the surface and diffuse across the Ni surface at a much higher rate than into the Ni bulk. If the deposition rate is large enough and the temperature is not too high, as to make diffusion into the bulk very likely, then the adsorbed C atoms should form dimers instead of being absorbed. Because dimers are more stable than monomers, they will not break unless the temperature is very high, nor will they diffuse into the bulk. Dimers may form trimers with the income of a third C atom or even diffuse across the surface with a somewhat higher activation energy of around 0.6 eV. Therefore, the formation of a monolayer will depend mostly on a delicate balance of the deposition rate and the temperature. We also note that the formation of a carbon cluster on Ni(111) is favored by symmetry (see Figure 6), since Ni(111) has a surface with hexagonal regularity and a lattice parameter very close to that of 1-LG.

Following the work by Ozcelik *et. al.* [31], it is possible that the atoms attached to the edges of the clusters will form pentagons and heptagons that will grow and heal themselves forming hexagons by a Stones-Wales-Thrower mechanism. Moreover, we suggest that the connection among the several nucleation centers may also happen through this process. For all this, we expect the 111 direction to provide the best quality graphene. With respect to the role of temperature, we propose that when it is low (800 ℃), there will be a high concentration of atomic carbon diffusing on the surface, but very little dimer diffusion and monomer diffusion into the bulk, so that eventually M-LG is going to grow. For higher temperatures (1000 ℃), however, diffusion into will occur more often for the individual carbon atoms generated on the surface, and less surface carbon concentration is expected. At the same time, dimer diffusion is going to become more probable, and those dimers could help the ordering to generate a 1-LG. Finally, if the temperature is too high (1100 ℃) the fast reactivity of CH_4 will generate a high carbon concentration at the surface. Diffusion into will saturate the bulk very quickly, and segregation will start to occur as well. M-LG is growing under these conditions. Although our calculations suggest that the growth of nucleation centers goes by the formation of dimers, the way such dimers would diffuse and contribute to the formation of nucleation centers was unclear until recently: Patera *et. al.* [68] demonstrated via experiments and DFT calculations that the 1-LG growth process occurs by the addition of carbon lines parallel to the graphene edge always involving a kink site and a Ni adatom. The participation of Ni adatoms is energetically favored since it reduces by about 35% the rate limiting energy barriers of the formation process (according to their calculations it lowers from 2.46 to 1.61 eV). Therefore, Ni adatoms, which spontaneously bind to kink sites in the graphene edge, act as single atom catalysts; carbon atoms stabilize the attachment of Ni adatoms, which consequently promotes the addition of carbon atoms in the edge formation. With basis in our calculations, we believe that, even though the range of temperatures in our experiments is different, the formation of graphene domains in our case should most likely follow the same trends.
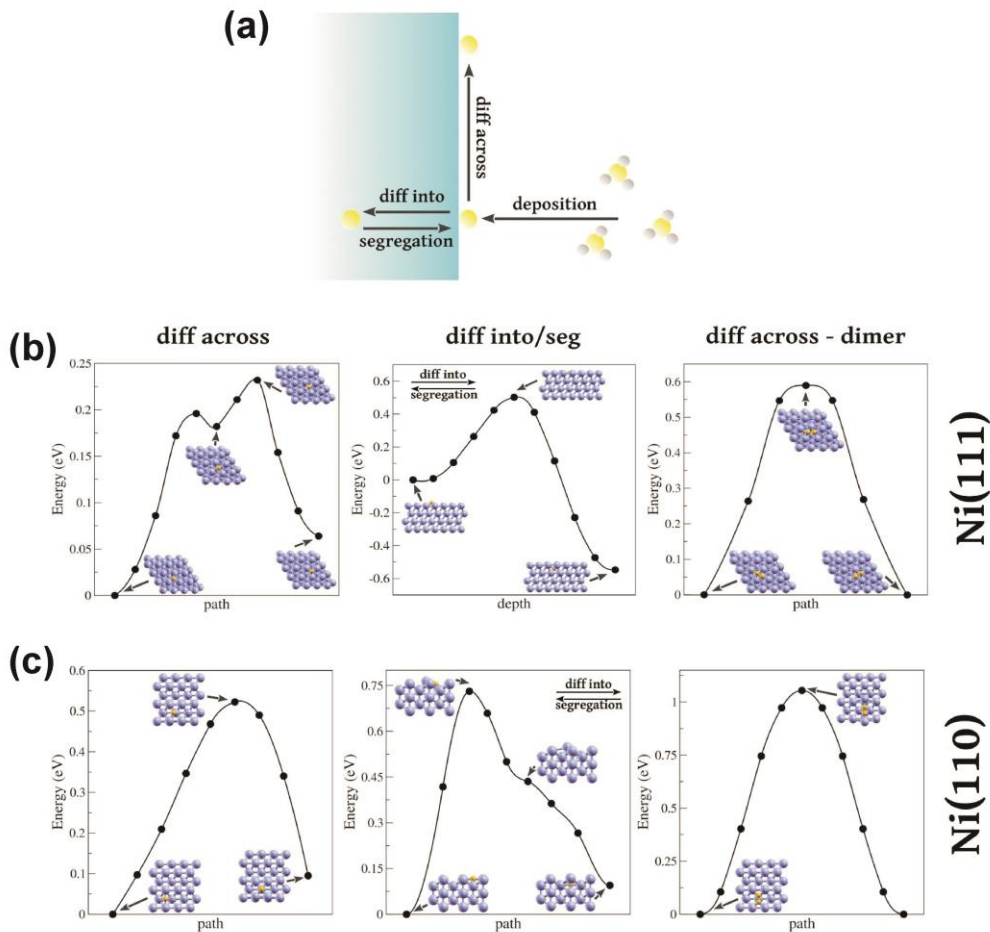
Figure 7 | Diffusion of carbon on a nickel surface. In (a) all the processes involved at the first stages of graphene growth on nickel are depicted. In (b) and (c) the kinetic barriers for diffusion across and into (or segregation, in reverse) for a single carbon atom and diffusion across for a dimer, on the 111 and 110 planes, are shown. The color code is the same as in Figure 5. For the case of Ni(100) all the barriers are higher than 1 eV, so they are not shown.

Growth of 1-LG on Ni(110):

Although the literature discusses that C-C bonds and monolayer graphene will be formed in this 110 direction, the understanding of the routes leading to the formation of a stable and large area of a graphene monolayer has been elusive [1-5,13-15,38, 43]. The Ni(110) crystallographic direction presents the surface with the lowest atomic packing density. The C deposition rate $(R_{Ni(110)})$ and the surface energy for Ni(110) are the largest compared to the 111 and 100 directions. In our experiments for Ni(110), by keeping the gas flow of H_2 and CH_4 at 1000 sccm and 100 sccm, respectively, and using a fast cooling down of the sample, 1-LG was obtained at

Comment [PA2]: Is it the lowest?

12

(800±1) $^{\circ}$C, M-LG was obtained at (1000±1) $^{\circ}$C and (1100±1) $^{\circ}$C and no carbon structure formation was observed below 800 $^{\circ}$C (see Table 1).

It is important to comment that the resulting 1-LG will be incommensurate with the Ni(110) surface. Indeed, Moiré patterns were already observed for 1-LG grown in Ni(110), which are signatures of incommensurate growth [13, 14]. Also, at different positions over the Ni(110) surface the carbon nucleation centers may acquire different orientations and graphene domains would start growing in diverse directions. As a consequence, we would expect graphene with poorer quality relative to that grown on the 111 plane. Indeed, the Raman spectrum in Figure 1f shows a significant D-band intensity for 1-LG grown on Ni(110), while Figure 1e shows a very weak D-band intensity for 1-LG grown on Ni(111). Our computer simulations suggest that the graphene monolayer formed on a perfect Ni(110) surface is not planar, but has a buckling due to the different C-Ni bonds formed. This difference has to do with the mismatch between the two structures. The best configuration found is shown in Figure 5, and the energetics and structural data are shown in Table 2. To the best of the authors' knowledge, a proposition of a model that consistently describes the dynamics of 1-LG formation in Ni(110) is still missing, although the information regarding diffusion and segregation is now becoming available [1,15].

Suggested Model for carbon growth on Ni(110):
Our computer simulations results suggest that carbon atoms would preferably attach to a bridge-001 site (see Figures 6 and S1 for details). The carbide formation is slightly disfavoured, but only by 0.09 eV. On this plane, the energy barriers to diffuse across and into are closer (0.53 and 0.72 eV, respectively), and we expect these two processes to compete more compared to the 111 case. Paths and kinetic barriers are shown in Figure 7c. The arrival of a second C atom creates a competition between dimer formation and isolated adsorption since they have very similar energies, as shown in Figure 6. ==Trimers and tetramers are less stable than dimers and are not likely to be formed==. Therefore, at the low coverage regime, the 110 face shows a more balanced thermodynamics, with dimer formation, diffusion and segregation in close competition with each other.

The incommensurability of graphene with the substrate may enforce growth through the healing mechanism of pentagons and heptagons [31]. On the other hand, the lack of hexagonal symmetry of this face may provoque that graphene domains growing from different nucleation sites join with different orientations. As a consequence, we would expect graphene with poorer quality relative to the 1-LG grown on the 111 direction. Electrical measurements should also confirm these statements about the quality of the 1-LG grown on the different Ni surfaces. However, to the best of the authors' knowledge, there are no such measurements in the literature focusing on the quality of graphene formed in each direction.

In summary, we suggest that a carbon on the 110 plane can diffuse across or into the bulk; the barriers for both processes are close, and the two of them should have a somewhat similar probability to occur. At low temperature (800℃) this balance allows the surface to have a moderate carbon concentration with enough time to order. Also the bulk should not saturate, and segregation is not likely to occur. Dimers are slightly less stable than monomers, so atomic

carbon is available to diffuse into the bulk while carbon concentration is low. After reaching some coverage, carbon atoms will start to join creating dimers and graphene would grow. The symmetry of the plane does not favour the formation of highly ordered graphene. When temperature is increased (1000ºC) the rate of CH_4 breaking increases. The bulk is saturated easily and segregation will occur. This high carbon concentration produces M-LG formation.

Growth of M-LG on Ni(100):

Epitaxial growth of 1-LG is not expected to happen due to the mismatch between graphene and Ni(100) surface basal planes. The C deposition rate ($R_{Ni(100)}$) and the surface energy for Ni(100) are smaller compared to the 110 direction but are larger compared to the 111 direction. Our computer simulations predict that, if formed, a graphene layer on the Ni(100) surface would not remain planar, but would present a strongly corrugated pattern mainly due to the mismatch between the two structures (graphene has a honeycomb structure while the Ni(100) surface has a square symmetry). These undulations prevent some of the carbon atoms to be directly linked to the metallic surface, as shown in Figure 5. In our experiments, even though we tested different growth parameters, such as temperature and gas flow, 1-LG was never obtained on Ni(100). To grasp why graphene is not formed, we need to understand better how carbon interacts with the Ni atoms at the surface when adsorbed or segregated.

We performed DFT calculations of the adsorption energy of individual carbon atoms on the 100 plane, finding that the most stable site is the hollow one (see Figures 6 and S1 for details). Observing the charge density difference plots (displayed in Figure 6) and Bader charges for the three surface planes (-0.70 for C on Ni(111), -0.83 for C on Ni(110) and -0.99 for C on Ni(100)), we can deduce that the C-Ni bonds on the 100 face are stronger and more localized than on the 111 and 110 planes. This charge localization would inhibit dimer formation, due to the fact that this new C-C bond would weaken the strong C-Ni and Ni-Ni already existing bonds. This disruption in the nickel orbitals (related to spin unpairing) would take the Ni crystal out of its energy minimum [1-5, 28, 38, 40, 41]. In fact, our calculations show that the dimer formation is highly unlikely at low coverages (dimer formation is 2.38 eV higher in energy than two carbon atoms separately adsorbed), which is also prevented by symmetry.

On the other hand, the large adsorption energy difference between sites (all listed in Table S1) makes lateral diffusion really difficult, with barriers in the order of 2.17 eV. Finally, although the 100 surface is more open than the 111 plane, diffusion into would not be likely to occur in the low coverage regime, and this is because the carbide (the carbon atom below the surface) is very unstable (1.15 eV higher in energy than a carbon on a surface hollow site). However, we expect that at high coverages carbon would be able to enter the surface and create lattice disorder. The fact that dimers are not likely to form is in agreement with previous experiments investigating segregation of carbon on Ni(100) surfaces; according to them, the monomers are well described by the Langmuir model, in which only non-interacting solute atoms are taken into account [1-5, 28, 38, 40, 41, 45]. Moreover, according to Porter et. al [1], segregation of C atoms to the surface of Ni(100) is reversible at monolayer coverages which is also a confirmation that C atoms at the surface are not interacting much with each other (or are only weakly interacting).

Comment [PA3]: We have to define low and high coverages.

14

It is important to mention that, most of the theoretical predictions [1-5, 9, 20, 30, 31] point out that Ni(100) is unlikely to allow any formation of an organized carbon structure. The authors, however, demonstrate in this manuscript that at high carbon saturation levels, which often happen at sufficiently high temperatures (above 800 ^{o}C in this work), M-LG structures exist on this face. The process behind such M-LG formation could be gather as follows: as the carbon coverage increases by CH_4 breaking, Ni bulk gets saturated as the diffusion into bulk of C atoms is favoured when compared to the segregation process. After saturation, while the fast cooling down process is happening, C atoms will segregate to the surface until the system Ni(100) + C reaches equilibrium. When this happens, the very last atoms to segregate will reach those already attached to the hollow sites of Ni(100), weakening their bonds with the metal. This C-Ni weakening may allow C-C bond formation. Ataca et. al [16] recently investigated theoretically the possibility that C linear chains may be formed on top of C atoms deposited on other surfaces. These C linear chains could be the starting point for the growth of M-LG on Ni(100).

In summary, after CH_4 breaking at the 100 surface, the carbon atoms attach strongly on the hollow sites (tetra-coordinated). These bonds are highly localized. Diffusion across and into are not likely to occur in the low coverage regime, because the barriers are very high. Dimers would not form, because the C-Ni bond is too strong when compared with a possible C-C bond. As the carbon concentration increases all the processes would start to compete. Some of the atoms would diffuse into the surface, and others would attach to the pre-existing Ni-C layer. When saturation is reached, segregated C atom would attach to the surface carbon layer from below. The plane symmetry and the high carbon concentration (even at low temperatures) will favor the precipitation of M-LG.

Growth of 1-LG on Ni(100) Thin Films:
Rasuli et. al [15] performed theoretical calculations simulating CVD growth of graphene on Ni(100). They predict that by varying the flux of gases and temperatures it is possible to grow high-quality monolayer graphene. In the present work, we varied the temperature until (1100±1) ^{o}C and varied the gas flux but we did not observe any carbon monolayer structure formation for the 1mm thick Ni(100) single crystals. A possibility to explain why their calculations predicted monolayer formation (and not multilayer formation) could be related to the fact that only four layers of Ni were used to represent the substrate, which may not be a good approximation. Moreover, in their calculation, strong Ni-C interactions may be underestimated at the low coverage regime, which appears from our findings to be fundamental to correctly predict the formation of carbon structures using a Ni(100) catalyst.

More recently, Zou *et. al.* [69] demonstrated via experiments and DFT calculations the successful growth of 1-LG in 1μm thick Ni(100) single crystals and in Ni(100) domains of 1μm thick polycrystalline Ni(100). Their calculations assume the interaction of a pre-existent monolayer with the Ni surface and are in good agreement with ours, as shortly described above. The experiments by Zou and colleagues [69] encouraged us to perform experiments in Ni(100) thin films as well. The growth conditions were the same described in the methods section. For the same gases and flow rates (H_2=1000 sccm, CH_4=100 sccm) and growth time (t=5 min), we

successfully obtained 1-LG in Ni(100) films with thickness around 1μm after fast cool down from a growth temperature of 1000 °C. Note that our results complement their findings since the growth temperature and the carbon source used here are different: their growth temperatures range from 400 to 600 °C and they use ethylene (C_2H_4) as a carbon source [69]. Figures 8(a) through (c) summarize our analysis of the 1-LG obtained from 1μm Ni(100) films, which are in good agreement with the analysis of the 1-LG obtained from Ni(111) and Ni(110), as discussed above.

The elucidation of the differences between thick and thin Ni films that lead to successful monolayer growth in thin films is an ongoing work that will be reported elsewhere. However, we would like to provide some preliminary insights that could explain such differences: the Ni(100) thin films might present different properties when compared with thicker Ni(100) films because, for example, the top and bottom surfaces are likely not isolated from one another anymore and may mutually interact. Therefore, the energy renormalizations related to the C-Ni and Ni-Ni bonds would no longer be local. This could change the activation energies for the diffusions into bulk and across the surface, the surface energies and adsorption energies.
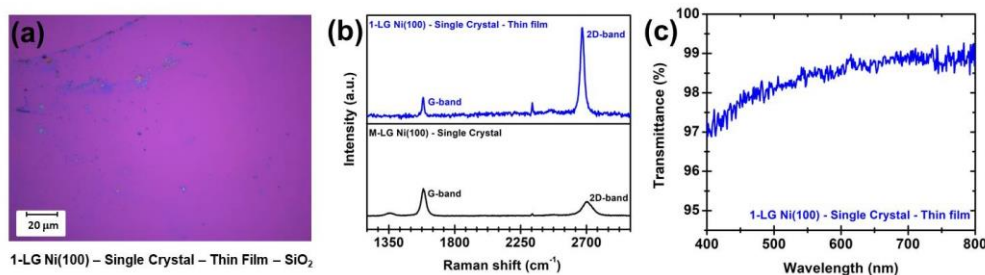

Figure 8 | (a) Optical image of the 1-LG obtained for Ni(100) films with thickness around 1μm using fast cool down approaches starting at T=1000 °C. (b) Top panel: Raman spectrum of the 1-LG imaged in (a). Bottom panel: for comparison, the Raman spectrum of the M-LG obtained for the Ni(100) single crystal discussed in the previous section. (c) Optical transmittance across the wavelength range of 400-800 nm for 1-LG films grown from 1μm thick Ni(100) films.

Non-occurrence of carbon structures at low temperatures (T<800 °C):

For the three studied crystallographic directions, no carbon structures were grown below 800 °C for the set of parameters used in our experiment, which keep the gas flow of H_2 and CH_4 at 1000 sccm and 100 sccm, respectively, and a fast cooling down of the sample. The authors understand that this situation is strongly connected to the decrease in the methane reactivity rate as the temperature decreases along with the cool down rates used in the experiments. Namely, a decrease in temperature of about 200 °C results in the decrease of CH_4 reactivity by more than an order of magnitude [26]. One way to overcome this decreased reactivity would be to increase the exposure time of the Ni surfaces to CH_4 (or equivalently, to increase the concentration of CH_4, which increases the probability for the molecule to be catalyzed). Another way would be to use other hydrocarbons. In fact, there have been numerous earlier reports on graphene growth at temperatures lower than 800 °C on Ni surfaces when other hydrocarbons

16

are used [13, 14, 46, 47]. As a last comment, even though diffusion into the bulk, diffusion across the surface and segregation also dramatically decrease below 800 ^{o}C, we do not believe that this is the main cause for the non-occurrence of carbon structures, since they have been observed to happen at temperatures as low as 350 ^{o}C. [1, 16]

CONCLUSIONS

In this combined experimental-theoretical study, we have demonstrated that Ni(111) and Ni(110) can be efficiently used to grow single-layer graphene (1-LG) under ambient pressure CVD, over areas on the order of a few cm^2. The formed graphene can be transferred to dielectric substrates, and our measurements using several techniques confirm the presence of 1-LG on Ni(111) and Ni(110). We have shown that, using the same gas flow rates and growth times, different temperatures are needed to grow 1-LG on Ni(111) (T=(1000±1) ^{o}C) and on Ni(110) (T=(800±1) ^{o}C). We have also performed DFT calculations to suggest atomistic models to explain the growth of graphene on the different facets. We propose that crystal symmetry, adsorption energies, diffusion across, diffusion into, segregation, and dimer formation are the key factors needed to formulate the explanations behind the first stages of the growth mechanisms. For Ni(100) we understand that the formation of 1-LG is not favored by symmetry and also by the very strong and localized Ni-C bonds, which do not favour the C-C dimer formation. However, we show that M-LG can be formed on Ni(100), in disagreement with previous predictions suggesting that organized carbon structures in this facet were unlikely or not possible. Therefore our discussion is very relevant to current research efforts in graphene fabrication and applications, especially when low temperature growth is desirable. Although only M-LG was possible for 1mm thick Ni(100) single crystals, 1-LG was successfully obtained for 1μm thick thin films, which complements recent results by Zou *et. al.* [69]. Due to the ease of multilayer growth on Ni, this study shows promise for extension to control the number of layers formed on different Ni surfaces, which can be beneficial for different technological applications. Finally, the next steps on this topic would be to perform detailed experiments to trace a map of thermodynamic parameters for the controllable growth of 1-LG in Ni(111) and Ni(110). For several different gases (H$_2$ and CH$_4$) flow rates, the strategy would consist on: (1) varying the growth temperatures; (2) for each growth temperature, varying the gases exposition time, which would control the deposition rates; (3) for each temperature and exposition time, experimenting different cooling down rates and (4) with such thermodynamic map, it is important to extend it for the controllable growth of n-LG (for n = 2, 3,…).

AUTHOR INFORMATION
*Corresponding authors:
paulo.t.araujo@ua.edu, f.ribeiro@ufabc.edu.br, jimenaolmos@gmail.com

Formatted: English (U.S.)

REFERENCES

[1] Blakely, J. M.; Kim J. S.; Potter, H. C. (1970) Segregation of Carbon to the (100) Surface of Nickel. J. Appl. Phys. 41 (6): 2693-2697.

[2] Isett, L. C.; Blakely, J. M. (1975) Binding energies of carbon to Ni(100) from equilibrium segregation studies. Surface Science 47 (2): 645-649.

[3] Isett, L. C.; Blakely, J. M. (1976) Segregation isosteres for carbon at the (100) surface of nickel. Surface Science 58 (2): 397-414.

[4] Schouten, F. C.; Gijzeman, O. L. J.; Bootsma, G. A. (1979) Interaction of Methane with Ni(111) and Ni(100); Diffusion of Carbon into Nickel through the (100) Surface; an AES-LEED Study. Surface Science 87 (1): 1-12.

[5] Shelton, J. C.; Patil, H. R.; Blakely, J. M. (1974) Equilibrium segregation of carbon to a nickel (111) surface: A surface phase transition. Surface Science 43 (2): 493-520.

[6] Li, X.; Cai, W.; Colombo, L.; Ruoff, R. S. (2009) Evolution of Graphene Growth on Ni and Cu by Carbon Isotope Labeling. Nanoletters 9 (12): 4268-4272.

[7] Yu, Q.; Lian, J.; Siriponglert, S.; Li, H.; Chen, Y. P.; Pei, S.-S. (2008) Graphene segregated on Ni surfaces and transferred to insulators. Applied Physics Letters 93 (11): 113103-3.

[8] Siegel, D. J.; Hamilton, J. C. (2005) Computational Study of Carbon Segregation and Diffusion within a Nickel Grain Boundary. Acta Macterialia 53 (1): 87-96.

[9] Kozlov, S. M.; Vines, F.; Goerling, A. (2011) Bonding Mechanisms of Graphene on Metal Surfaces. J. Phys. Chem. C 116 (13): 7360-7366.

[10] Cepek, C.; Goldoni, A.; Modesti, S. (1996) Chemisorption and Fragmentation of C60 on Pt(111) and Ni(110). Phys. Rev. B 53 (11): 7466-7472.

[11] Foiles, S. M.; Baskes, M. I.; Daw, M. S. (1986) Embedded-atom-method Functions for the fcc Metals Cu, Ag, Au, Ni, Pd, Pt, and their Alloys. Phys. Rev. B 33 (12): 7983-7991.

[12] Foiles, S. M. (1985) Calculation of the Surface Segregation of Ni-Cu Alloys with the use of the Embedded-atom Method. Phys. Rev. B 32 (12): 7685-7693.

[13] Usachov, D.; Dobrotvorskii, A. M.; Varykhalov, A.; Rader, O.; Gudat, W.; Shikin, A. M.; Adamchuk, V. K. (2008) Experimental and theoretical study of the morphology of commensurate and incommensurate graphene layers on Ni single-crystal surfaces. Phys. Rev. B 78 (8): 085403.

[14] Fedorova, A. V.; Varykhalovb, A. Yu.; Dobrotvorskiia, A. M.; Chikinaa, A. G.; Adamchuka, V. K.; Usachova, D. Yu. (2011) Structure of Graphene on the Ni(110) Surface. Physics of the Solid State 53 (9): 1952-1956.

[15] Rasuli, R.; Mostafavi, Kh.; Davoodi J. (2014) Molecular dynamics simulation of graphene growth on Ni(100) facet by chemical vapor deposition. J. of Appl. Phys. 115 (2): 024311.

[16] Ataca, A.; Ciraci, S. (2011) Perpendicular Growth of Carbon Chains on Graphene from First-Principles. Phys. Rev. B 83 (23): 235417.

[17] Reina, A.; Jia, X.; Ho, J.; Nezich, D.; Son, H.; Bulovic, V.; Dresselhaus, M. S.; Kong, J. (2009) Large Area, Few-Layer Graphene Films on Arbitrary Substrates by Chemical Vapor Deposition. Nanoletters 9 (1): 30-35.

[18] De Arco, L. G.; Yi, Z.; Kumar, A.; Chongwu, Z. (2009) Synthesis, Transfer, and Devices of Single- and Few-Layer Graphene by Chemical Vapor Deposition. Nanotechnology, IEEE Transactions 8 (2): 135-138.

[19] Kim, K. S.; Zhao, Y.; Jang, H.; Lee, S. Y.; Kim, J. M.; Kim, K. S.; Ahn, J.-H.; Kim, P.; Choi, J.-Y.; Hong, B. H. (2009) Large-scale pattern growth of graphene films for stretchable transparent electrodes. Nature 457 (7230): 706-710.

[20] Isett, L. C.; Blakely, J. M. (1975) Binding of carbon atoms at a stepped - Ni surface. Journal of Vacuum Science and Technology 12 (1): 237-241.

[21] Gamo, Y.; Nagashima, A.; Wakabayashi, M.; Terai, M.; Oshima, C. (1997) Atomic structure of monolayer graphite formed on Ni(111). Surface Science 374 (1-3): 61-64.

[22] Seung Jin, C.; Fethullah, G.; Scedil; Ki Kang, K.; Eun Sung, K.; Gang Hee, H.; Soo Min, K.; Hyeon-Jin, S.; Seon-Mi, Y.; Jae-Young, C.; Min Ho, P.; Cheol Woong, Y.; Didier, P.; Young Hee, L. (2009) Synthesis of Large-Area Graphene Layers on Poly-Nickel Substrate by Chemical Vapor Deposition: Wrinkle Formation. Advanced Materials 21 (22): 2328-2333.

[23] Reina, A.; Thiele, S.; Jia, X.; Bhaviripudi, S.; Dresselhaus, M.; Schaefer, J.; Kong, J. (2009) Growth of large-area single- and Bi-layer graphene by controlled carbon precipitation on polycrystalline Ni surfaces. Nano Research 2 (6): 509-516.

[24] Nair, R. R.; Blake, P.; Grigorenko, A. N.; Novoselov, K. S.; Booth, T. J.; Stauber, T.; Peres, N. M. R.; Geim, A. K. (2008) Fine Structure Constant Defines Visual Transparency of Graphene. Science 320 (5881): 1308.

[25] Bengaard, H. S.; Nørskov, J. K.; Sehested, J.; Clausen, B. S.; Nielsen, L. P.; Molenbroek, A. M.; Rostrup-Nielsen, J. R. (2002) Steam Reforming and Graphite Formation on Ni Catalysts. Journal of Catalysis 209 (2): 365-384.

[26] Beebe, T. P.; Goodman, D. W.; Kay, B. D.; Yates, J. T. (1987) Kinetics of the activated dissociative adsorption of methane on the low index planes of nickel single crystal surfaces. The Journal of Chemical Physics 87 (4): 2305-2315.

[27] Lander, J. J. ; Kern, H. E.; Beach, A. L. (1952) Solubility and Diffusion Coefficient of Carbon in Nickel: Reaction Rates of NickelCarbon Alloys with Barium Oxide. Journal of Applied Physics 23 (12): 1305 -1309.

[28] Novoselov, K. S.; Geim, A. K.; Morozov, S. V.; Jiang, D.; Zhang, Y.; Dubonos, S. V.; Grigorieva, I. V.; Firsov, A. A. (2004) Electric Field Effect in Atomically Thin Carbon Films. Science 306 (5696): 666-669.

[29] Herbig, M.; Raabe, D.; Li, Y. J.; Choi, P.; Zaefferer, S,; Goto, S. (2014) Atomic-Scale Quantification of Grain Boundary Segregation in Nanocrystalline Material. Phys. Rev. Lett. 112 (12): 126103.

[30] Zangwill, A.; Vvedensky, D. D. (2011) Novel Growth Mechanism of Epitaxial Graphene on Metals. Nanoletters 11 (5): 2092-2095.

[31] Ozcelik, V. O.; Cahangirov, S.; Ciraci, S. (2012) Epitaxial Growth Mechanisms of Graphene and Effects of Substrates. Phys. Rev. B 85 (23): 235456.

[32] Li, X.; Cai, W.; An, J.; Kim, S.; Nah, J.; Yang, D.; Piner, R.; Velamakanni, A.; Jung, I.; Tutuc, E.; Banerjee, S. K.; Colombo, L.; Ruoff, R. S. (2009) Large-Area Synthesis of High-Quality and Uniform Graphene Films on Copper Foils. Science 324 (5932): 1312-1314.

[33] Bae, S.; Kim, H.; Lee, Y.; Xu, X.; Park, J.-S.; Zheng, Y.; Balakrishnan, J.; Lei, T.; Ri Kim, H.; Song, Y. I.; Kim, Y.-J.; Kim, K. S.; Ozyilmaz, B.; Ahn, J.-H.; Hong, B. H.; Iijima, S. (2010) Roll-to-roll production of 30-inch graphene films for transparent electrodes. Nature Nanotechnology 5 (8): 574–578.

[34] Bhaviripudi, S; Jia, X; Dresselhaus, M. S.; Kong, J. (2010) Role of Kinetic Factors in Chemical Vapor Deposition Synthesis of Uniform Large Area Graphene Using Copper Catalyst. Nanoletters 10 (10): 4128–4133.

[35] Lahiri, J.; Lin, Y.; Bozkurt, P.; Oleynik, I. I.; Batzill, M. (2010) An extended defect in graphene as a metallic wire. Nature Nanotechnology 5 (5): 326.

[36] Li, X.; Zhu, Y.; Cai, W.; Borysiak, M.; Han, B.; Chen, D.; Piner, R. D.; Colombo, L.; Ruoff, R. S. (2009) Transfer of Large-Area Graphene Films for High-Performance Transparent Conductive Electrodes. Nanoletters 9 (12): 4359-4363.

[37] Landau, L. D.; Lifshitz, E. M. (1986) Theory of Elasticity - Third Edition. Pergamon Press.

[38] Chen, H.; Zhu, W.; Zhang, Z. (2010) Contrasting Behavior of Carbon Nucleation in the Initial Stages of Graphene Epitaxial growth on Stepped Metal Surfaces. Phys. Rev. Lett. 104 (18): 186101.

[39] Weatherup, R. S.; Bayer , B. C.; Blume , R.; Ducati, C.; Baehtz , C.; Schlögl , R.; Hofmann, S. (2011) In Situ Characterization of Alloy Catalysts for Low-Temperature Graphene Growth. Nanoletters 11 (10): 4154–4160.

[40] McQuarrie, D. A. (1976) Statistical Mechanics - First Edition. Harper and Row.

[41] Wise, H.; Oudar, J. (2001) Materials Concepts in Surface Reactivity and Catalysis. Dover Publications, NY.

[42] Gonis, A.; Meike, A.; Turchi, P. E.A. (1996) Properties of Complex Inorganic Solids; Plenum, New York, US.

[43] Murata, Y.; Petrova, V.; Kappes, B. B.; Ebnonnasir, A.; Petrov, I.; Xie, Y.-H. ; Ciobanu, C. V.; Kodambaka, S. (2010) Moiré Superstructures of Graphene on Faceted Nickel Islands. ACS Nano 4 (11): 6509-6514.

[44] Papagno, L.; Caputi, L. S. (1984) Determination of graphitic carbon structure adsorbed on Ni(110) by surface extended energy-loss fine-structure analysis. Phys. Rev. B 29: 1483.

[45] Wiltner, A; Linsmeier, Ch.; Jacob, T. (2008) Carbon reaction and diffusion on Ni(111), Ni(100), and Fe(110): Kinetic parameters from x-ray photoelectron spectroscopy and density functional theory analysis. J. Chem. Phys. 129 (8): 084704.

[46] Muñoz, R.; Gómez-Aleixandre, C. (2013) Review of CVD Synthesis of Graphene. Chem. Vap. Deposition 19: 297-322.

[47] Zhang, Y.; Zhang, L.; Zhou, C. (2013) Review of Chemical Vapor Deposition of Graphene and Related Applications. Acc. Chem. Res. 46 (10): 2329-2339.

[48] Wang, Y.; Zheng, Y.; Xu, X.; Dubuisson, E.; Bao, Q.; Lu, J.; Loh, K. P. (2011) Electrochemical Delamination of CVD-Grown Graphene Film: Toward the Recyclable Use of Copper Catalyst. ACS Nano 5 (12): 9927-9933.

[49] Gao, L.; Ren, W.; Xu, H.; Jin, L.; Wang, Z.; Ma, T.; Ma, L.-P.; Zhang, Z.; Fu, Q.; Peng, L.-M.; Bao, X.; Cheng, H.-M. (2012) Repeated growth and bubbling transfer of graphene with millimetre-size single-crystal grains using platinum. Nat. Commun. 3: 1.

[50] Mafra, D. L.; Ming, T.; Kong. J. (2015) Facile graphene transfer directly to target substrates with a reusable metal catalyst. Nanoscale 7: 14807.

[51] Dahal, A.; Batzill, M. (2014) Graphene–nickel interfaces: a review. Nanoscale 6: 2548.

[52] Xu, Z.; Yan, T.; Liu, G.; Qiao, G.; Ding, F. (2016) Large scale atomistic simulation of single-layer graphene growth on Ni(111) surface: molecular dynamics simulation based on a new generation of carbon–metal potential. Nanoscale 8: 921.

[53] Delamoreanu, A.; Rabot, C.; Vallee, C.; Zenasni, A. (2014) Wafer scale catalytic growth of graphene on nickel by solid carbon source. Carbon 66: 48.

[54] Wu, T.; Zhang, X.; Yuan, Q.; Xue, J.; Lu, G.; Liu, Z.; Wang, H.; Wang, H.; Ding, F.; Yu, Q.; Xie, X.; Jiang, M. (2016) Fast growth of inch-sized single-crystalline graphene from a controlled single nucleus on Cu–Ni alloys. Nat. Mater. 15: 43.

[55] Garlow, J. A.; Barrett, L. K.; Wu, L.; Kisslinger, K.; Zhu, Y.; Pulecio, J. F. (2016) Mechanisms of graphene growth by chemical vapour deposition on transition metals. Sci. Rep. 6: 19804.

[56] Seah, C-M.; Vigolo, B.; Chai, S-P.; Ichikawa, S.; Gleize, J.; Le Normand, F.; Aweke, F.; Mohamed, A. R. (2016) Sequential synthesis of free-standing high quality bilayer graphene from recycled nickel foil. Carbon 96: 268.

[57] Ren, Z.; Meng, N.; Shehzad, K.; Xu, Y.; Qu, S.; Yu, B.; Luo, J. K. (2015) Mechanical properties of nickel-graphene composites synthesized by electrochemical deposition. Nanotechnology 26: 065706.

[58] Hohenberg, P.; Kohn, W. (1964) Inhomogeneous Electron Gas. Phys. Rev. 136:B864–B871.

[59] Giannozzi, P.; Baroni, S.; Bonini, N.; Calandra, M.; Car, R.; Cavazzoni, C.; Ceresoli, D.; Chiarotti, G. L.; Cococcioni, M.; Dabo, I.; Dal Corso, A.; Fabris, S.; Fratesi, G.; de Gironcoli, S.; Gebauer, R.; Gerstmann, U.; Gougoussis, C.; Kokalj, A.; Lazzeri, M.; Martin-Samos, L.; Marzari, N.; Mauri, F.; Mazzarello, R.; Paolini, S.; Pasquarello, A.; Paulatto, L.; Sbraccia, C.; Scandolo, S.; Sclauzero, G.; Seitsonen, A. P.; Smogunov, A.; Umari, P.; Wentzcovitch, R. M.

22

(2009) QUANTUM ESPRESSO: a modular and open-source software project for quantum simulations of materials. J. Phys.:Condens. Matter 21: 395502.

[60] Perdew, J. P.; Burke, K.; Ernzerhof, M. (1996) Generalized Gradient Approximation Made Simple. Phys. Rev. Lett. 77:3865–3868.

[61] Dal Corso, A. (2014) Pseudopotentials periodic table: From H to Pu. Comput. Mater. Sci. 95: 337-350.

[62] Grimme, S.; (2006) Semiempirical GGA-type density functional constructed with a long-range dispersion correction. J. Comp. Chem. 27: 1787.

[63] Kittel, C. (2005) Introduction to Solid State Physics, 8th edition. John Wiley and Sons, NJ.

[64] Lee,B-J.; Shim, J-H.; Baskes, M. I. (2003) Semiempirical atomic potentials for the fcc metals Cu, Ag, Au, Ni, Pd, Pt, Al, and Pb based on first and second nearest-neighbor modified embedded atom method. Phys. Rev. B 68: 144112.

[65] Chung, Y. W. (2001) Practical Guide to Surface Science and Spectroscopy. Academic Press, CA.

[66] Bianchini, F.; Patera, L. L.; Peressi, M.; Africh, C.; Comelli, G. (2014) Atomic Scale Identification of Coexisting Graphene Structures on Ni(111). J. Phys. Chem. Lett. 5 (3): 467-473.

[67] Zhao, W.; Kozlov, S. M.; Höfert, O.; Gotterbarm, K.; Lorenz, M. P. A.; Viñes, F.; Papp, C.; Göling, A.; Steinrück, H-P. (2011) Graphene on Ni(111): Coexistence of Different Surface Structures. J. Phys. Chem. Lett. 2 (7): 759-764.

[68] Patera, L. L.; Bianchini, F.; Africh, C.; Dri, C.; Soldano, G.; Mariscal, M. M.; Peressi, M.; Comelli, G. (2018) Real-time imaging of adatom-promoted graphene growth on nickel. Science 359: 1243-1246.

[69] Zou, Z.; Carnevali, V.; Jugovac, M.; Patera, L. L.; Sala, A.; Panighel, M.; Cepek, C.; Soldano, G.; Mariscal, M. M.; Peressi, M.; Comelli, G.; Africh, C. (2018) Graphene on nickel (100) micrograins: Modulating the interface interaction by extended moiré superstructures. Carbon 130: 441-447.